

LAND USE AND LAND COVER CLASSIFICATION USING RADARSAT-2 POLARIMETRIC SAR IMAGE

Z. Qi^{a,*}, A. G. Yeh^a, X. Li^b, Z. Lin^b

^a Department of Urban Planning and Design, The University of Hong Kong, Pokfulam Road, Hong Kong SAR, P.R. China - qizhixin@hkusua.hku.hk

^b School of Geography and Planning, Sun Yat-sen University, 135 West Xingang Rd., Guangzhou 510275, P.R. China - lixia@mail.sysu.edu.cn

KEY WORDS: Land cover, Land user, Polarization, RADARSAT, SAR

ABSTRACT:

Traditional pixel-based classification methods yield poor results when applied to synthetic aperture radar (SAR) imagery because of the presence of the speckle and limited spectral information in SAR data. A novel classification method, integrating polarimetric target decomposition, object-oriented image analysis, and decision tree algorithms, is proposed for land use and land cover (LULC) classification using RADARSAT-2 polarimetric SAR (PolSAR) data. The new method makes use of polarimetric information of PolSAR data, and takes advantage of object-oriented analysis and decision tree algorithms. The polarimetric target decomposition is aimed at extracting physical information from the observed scattering of microwaves by surface and volume for the classification of scattering data. The main purposes of the object-oriented image analysis are delineating objects and extracting various features, such as tone, shape, texture, area, and context. Decision tree algorithms provide an effective way to select features and create a decision tree for classification. The comparison between the proposed method and the Wishart supervised classification was made to test the performance of the proposed method. The overall accuracies of this proposed method and the Wishart supervised classification were 89.34% and 79.36%, respectively. The results show that the proposed method outperforms the Wishart supervised classification, and is an appropriate method for LULC classification of RADARSAT-2 PolSAR data.

1. INTRODUCTION

LULC classification of PolSAR data has become an important research topic since PolSAR images through ENVISAT ASAR, ALOS PALSAR and RADARSAT-2 were available. Classification methods for PolSAR images have been explored by many researchers (Rignot et al., 1992; Chen et al., 1996; Barnes and Burki, 2006; Alberga, 2007). Recently some polarimetric decomposition theorems have been introduced (Cloude and Pottier, 1996; Freeman and Durden, 1998; Yang et al., 1998; Cameron and Rais, 2006), and classification methods based on the decomposition results were also explored by some researchers (Cloude and Pottier, 1997; Lee et al., 1999; Pottier and Lee, 2000; Ferro-Famil et al., 2001). The polarimetric decomposition is aimed at extracting physical information from the observed scattering of microwaves by surface and volume for the classification of scattering data. However, so far most of the classification methods for PolSAR images are pixel-based, and have limitations for representing objects in high-resolution images and difficulties to utilize the abundant information of PolSAR imagery. The performance of pixel-based classification methods is affected by speckles, and only tonal information of pixels can be used by these methods. Moreover, the results of the pixel-based methods are almost discontinuous raster format maps, which are hardly to use to extract objects of interest and update geographical information system database expediently.

In recent years, object-oriented image analysis has been increasingly used for the classification of remote sensing data (Evans et al., 2002; Geneletti and Gorte, 2003; Li, et al., 2008). By delineating objects from remote sensing images, the object-oriented analysis can obtain a variety of additional spatial and textural information, which is important for improving the accuracy of remote sensing classification (Benz et al., 2004). However, with the addition of spatial and contextual variables,

there are hundreds of features that can potentially be incorporated into the analysis. Therefore, feature selection can present a problem in object-based classification (Laliberte et al., 2006). Since recently some polarimetric decomposition theorems have been introduced, which brings abundant polarimetric information, the problems of feature selection become more intractable.

Decision tree algorithms can be used to solve the problems of feature selection. Decision trees are commonly used for variable selection to reduce data dimensionality in image analysis (Lawrence and Wright, 2001). Classification accuracies from decision tree classifiers are often greater compared to using maximum likelihood or linear discriminant function classifiers (Laliberte et al., 2006). Some studies have indicated that decision trees can provide an accurate and efficient methodology for classification of remote sensing data (Friedl and Brodley, 1997; Swain and Hauska, 1977; McIver and Friedl, 2002).

The objective of this study is to explore a new classification method of integrating polarimetric decomposition, object-oriented image analysis, and decision tree algorithms for PolSAR imagery. In this method, 39 polarimetric descriptors were first calculated by using the H/A/Alpha polarimetric decomposition and combined with the parameters of the scattering and coherency matrix to form a multichannel image. Next, during the object-oriented image analysis, image objects were delineated by implementing a multi-resolution segmentation on the Pauli composition image of RADARSAT-2 PolSAR data. Meanwhile, a total of 1253 features were extracted for each image object. Then, a decision tree algorithm was used to select features and create a decision tree for the classification. Finally, the LULC classification of RADARSAT-

* Corresponding author

2 PolSAR image was carried out by using the constructed decision tree.

2. METHODOLOGY

2.1 Polarimetric target decomposition

Target decomposition theorems were first formalized by Huynen (Huynen, 1970), and then many decomposition methods were proposed by other researchers. In this study we just focus on H/A/Alpha decomposition (Cloude and Pottier, 1997). The H/A/Alpha decomposition is also called eigenvector-eigenvalue based decomposition. This decomposition method is free from the physical constraints imposed by multivariate models because it is not dependent on the assumption of a particular underlying statistical distribution.

The most important observable measured by radar system is the 3×3 coherency matrix T_3 , and it is written as:

$$T_3 = \frac{1}{2} \begin{bmatrix} |S_{hh} + S_{vv}|^2 & (S_{hh} + S_{vv})(S_{hh} - S_{vv})^* & 2(S_{hh} + S_{vv})S_{hv}^* \\ (S_{hh} - S_{vv})(S_{hh} + S_{vv})^* & |S_{hh} - S_{vv}|^2 & 2(S_{hh} - S_{vv})S_{hv}^* \\ 2S_{hv}(S_{hh} + S_{vv})^* & 2S_{hv}(S_{hh} - S_{vv})^* & 4|S_{hv}|^2 \end{bmatrix} \quad (1)$$

where, S_{hh} and S_{vv} denote the copolarized complex scattering amplitudes; S_{hv} and S_{vh} denote the cross-polarized complex scattering amplitudes, respectively; * denotes conjugate, and | | denotes module.

According to the H/A/Alpha decomposition theorem, T_3 can be decomposed as follows:

$$T_3 = \begin{bmatrix} \underline{u}_1 & \underline{u}_2 & \underline{u}_3 \end{bmatrix} \begin{bmatrix} \lambda_1 & 0 & 0 \\ 0 & \lambda_2 & 0 \\ 0 & 0 & \lambda_3 \end{bmatrix} \begin{bmatrix} \underline{u}_1 & \underline{u}_2 & \underline{u}_3 \end{bmatrix}^T \quad (2)$$

where $\lambda_1, \lambda_2, \lambda_3$ are the eigenvalues of T_3 , and $\infty > \lambda_1 > \lambda_2 > \lambda_3 > 0$. \underline{u}_i for $i=1,2,3$ are the eigenvectors of T_3 and can be formulated as follows:

$$\underline{u}_i = \begin{bmatrix} \cos \alpha_i & \sin \alpha_i \cos \beta_i e^{j\delta_i} & \sin \alpha_i \cos \beta_i e^{j\delta_i} \end{bmatrix}^T \quad (3)$$

where, the symbol T stands for complex conjugate.

The pseudo-probabilities of the T_3 expansion elements are defined from the set of sorted eigenvalues.

$$p_i = \lambda_i / \sum_{k=1}^3 \lambda_k \quad \text{with} \quad p_1 \geq p_2 \geq p_3 \quad (4)$$

where p_i is called the probability of the eigenvalue λ_i and represents the relative importance of this eigenvalue to the total scattered power.

In general, the columns of the 3×3 unitary matrix U_3 are not only unitary but mutually orthogonal. This means that in

practice, the parameters $(\alpha_1, \alpha_2, \alpha_3)$, $(\beta_1, \beta_2, \beta_3)$, $(\delta_1, \delta_2, \delta_3)$, and $(\gamma_1, \gamma_2, \gamma_3)$ are not independent. Thus, each polarimetric parameter is associated with a three-symbol Bernoulli statistical process. In this way, the estimate of the mean polarimetric parameter set is given by (Lee and Poitter, 2009):

$$\overline{(\alpha, \beta, \gamma, \delta)} = \sum_{i=1}^3 p_i \cdot (\alpha_i, \beta_i, \gamma_i, \delta_i) \quad (5)$$

The eigenvalues and eigenvectors are the primary parameters of the eigenvector-eigenvalue based decomposition of T_3 . The different secondary polarimetric descriptors are defined as a function of the eigenvalue and eigenvectors of T_3 for simplifying the analysis of the physical information provided by this decomposition (Lee and Poitter, 2009):

1) Polarimetric scattering entropy (H)

The polarimetric scattering entropy defines the degree of statistical disorder of each distinct scatter type within the ensemble.

2) Polarimetric scattering anisotropy (A)

The anisotropy measures the relative importance of the second and the third eigenvalues of the eigen decomposition. It is a useful parameter to improve the capability to distinguish different types of scattering process.

3) Combinations between entropy (H) and anisotropy (A)

- The $(1-H)(1-A)$ image corresponds to the presence of a single dominant scattering process.
- The $H(1-A)$ image characterizes a random scattering process.
- The HA image relates to the presence of two scattering mechanisms with the same probability.
- The $(1-H)A$ image corresponds to the presence of two scattering mechanisms with a dominant process and a second one with medium probability.

4) SERD and DERD

Single bounce Eigenvalue Relative Difference (SERD) and the Double bounce Eigenvalue Relative Difference (DERD) are sensitive to natural media characteristics and can be used for quantitative inversion of bio- and geophysical parameters.

5) Polarization asymmetry (PA) and Polarization fraction (PF)

PF ranges between 0 and 1, when $\lambda_3=0$ the entire return is polarized, and when $\lambda_3>0$ the polarization fraction drops. The PA measures the relative strength of the two polarimetric scattering mechanisms.

6) Radar vegetation Index (RVI) and Pedestal height (PH)

The RVI was used for analyzing scattering from vegetated areas. The PH is another polarization signature of measuring randomness in the scattering.

7) Target randomness parameter (P_R)

P_R is very close to the entropy (H) and provides the similar information.

8) Shannon entropy (SE):

This parameter is a sum of SE_I and SE_p . SE_I is the intensity contribution that depends on the total backscattered power, and SE_p the polarimetric contribution that depends on the Barakat degree of polarization.

The information provided by the H/A/Alpha decomposition of the coherency matrix can be interrelated in terms of the eigenvalues and eigenvectors of the decomposition or in terms of secondary polarimetric descriptors. Both interpretations have to be considered as complementary. In this study, PolSARPro 4.0 software was used to implement the H/A/Alpha decomposition (López-Martínez, 2005).

2.2 Object-oriented image analysis

At present most of orbital radar images are obtained using only one single frequency. There are significant confusions if classification is purely based on a single band of SAR images (Li and Yeh, 2004). One way to compensate for the limited information of single frequency is to derive more features such as texture and shape for the classification beside of spectral information of radar images. Object-oriented image analysis can be used on radar images to extract such type of information. Such analysis is especially useful in improving the classification accuracy of high-resolution images (Langford, 2002).

There are two steps in the object-oriented analysis: (1) Image segmentation; (2) Feature extraction. In this study, multi-resolution segmentation was used to delineate objects based on shape and color homogeneity (Benz et al., 2004) from the Pauli composition image of RADARSAT-2 PolSAR data. Pauli composition has become today the standard for PolSAR image display, and thus it is often used for visual interpretation and observation. In order to obtain the best discrimination results, both color and shape heterogeneity is used to adjust the segmentation. The object-oriented package, Definiens Developer 7.0 (previously called eCognition), is used to implement the object-oriented image analysis.

The multi-resolution segmentation algorithm is a bottom up region-merging technique starting with one-pixel objects. During the region-merging process, smaller image objects are merged into bigger ones, and the underlying optimization procedure minimizes the weighted heterogeneity of resulting image objects for a given resolution over the whole scene. Heterogeneity is determined based on the standard deviation of color properties and their shapes. The merging of a pair of adjacent image objects leads to the smallest growth of the defined heterogeneity. The process will stop if the smallest growth exceeds the threshold defined by a scale parameter.

Various types of features can be obtained via object-oriented image analysis, such as mean value of pixels and standard deviation of pixels in an image object, mean difference to neighbors, area, length, GLCM Homogeneity, GLCM Contrast and so on. The interrelations among objects can be defined and utilized as additional information for classification.

2.3 Decision tree algorithm

The task of this work is to determine the class of each image object based on their features. Since a large set of features can be extracted from image objects, the selection of proper features is important for classification. Decision trees are commonly used for variable selection to reduce data dimensionality in image analysis (Lawrence and Wright, 2001). Decision trees are used to predict membership of cases or objects in the classes of a categorical dependent variable from their measurements on one or more predictor variables. In these tree structures, leaves represent classifications and branches represent conjunctions of features that lead to those classifications.

Decision tree algorithms have many advantages: (1) they are white box model and simple to understand and interpret. If a given result is provided by the model, the explanation for the result is easily replicated by simple math; (2) Decision trees are able to handle both numerical and categorical data, and requires little data preparation; (3) They are robust and perform well with large data in a short time; (4) Decision trees, performing univariate splits and examining the effects of predictors one at a time, have implications for the variety of types of predictors that can be analyzed.

In this study, QUEST was used to implement the LULC classification. The QUEST is a binary-split decision tree algorithm for classification and data mining (Loh and Shih, 1997). A decision tree can be created based on training samples using QUEST. After the decision tree is constructed, it can be used to identify the class of other unknown cases.

3. IMPLEMENTATIONS AND RESULTS

3.1 The study area and data processing

The study area is located in the Panyu District with latitudes 22°51' to 22°58' and longitudes 113°20' to 113°33' of Guangzhou in southern China. Panyu lies at the heart of the Pearl River Delta, and has a total land area of 1,314 km² and a population of 926,542. This district was an agricultural country before economic reform in 1978 but has been transformed recently into a rapidly urbanized area. Since Panyu became a district of Guangzhou in July 2000, intensive land development has occurred to provide housing to the residents of Guangzhou City. Huge profits have been generated through property development, which results in the increase of land speculation activities and illegal land development. Accurate and timely LULC information can provide government with scientific information for making management policies to control and prevent illegal developments at an early stage.

The RADARSAT-2 image with the fine quad-pol (FQ12) and Single Look Complex (SCL) obtained on 21 March 2009 was used in this study (Figure 1.). The image has a full polarization of HH, HV, VH and VV, a resolution of 5.2 × 7.6m and an incidence angle of 31.5 degrees. Data processing included radiometric calibration, geometric calibration, slant range to ground range and image filtering. Lee refined filter, which proves to be efficient in polarimetric SAR images, was applied to the RADARSAT-2 data.



Figure 1. RADARSAT-2 Quad-Pol image of the study area (Pauli Composition: HH+VV, HV, HH-VV)

The final LULC map displays categories including built-up area, water, barren land and vegetation. In field work, a total of 497 field plots were selected across typical LULC classes based on a

clustered sampling approach (McCoy, 2005). A suggestion by Congalton and Green (1999), based on experience with the multinomial distribution, is to use a minimum of 50 samples for each category. A minimum sample unit should be no smaller than 3×3 cluster of pixels or a polygon of comparable size for either training sites or accuracy assessment sites (McCoy, 2005). In this study, the sampling size per field plot ranged from 15 to 54 pixels, which was determined by the size of a ground photos taken concurrently. The collected field plots were divided into two groups for the training and validation. There were 210 plots in the training group and 287 plots in the validation group. The first group was used to select features and create a decision tree with QUEST for the classification, and the second group, which included 7520 pixels, was used to verify the results of the LULC classification. An ALOS image of the 10m multispectral bands obtained on 31 November 2008 was used as a reference map to assist the collection of ground true information.

3.2 Polarimetric target decomposition results

The H/A/Alpha decomposition was used to extract polarimetric descriptors from the RADARSAT-2 data. A total of 39 descriptors were extracted and combined with the elements of the scattering and coherency matrix to form a PolSAR multichannel image. The descriptors and the corresponding image channels are listed in Table 2.

Channel	Descriptor	Channel	Descriptor	Channel	Descriptor
1	HH	19	p_2	37	H
2	HV	20	p_3	38	A
3	VH	21	α	39	$(1-H)(1-A)$
4	VV	22	α_1	40	$(1-H)A$
5	HH+VV	23	α_2	41	$H(1-A)$
6	HV+VH	24	α_3	42	HA
7	HH-VV	25	β	43	SERD
8	T11	26	β_1	44	DERD
9	T12	27	β_2	45	PA
10	T13	28	β_3	46	PF
11	T22	29	δ	47	RVI
12	T23	30	δ_1	48	PH
13	T33	31	δ_2	49	P_R
14	$\bar{\lambda}$	32	δ_3	50	SE
15	λ_1	33	γ	51	SE ₁
16	λ_2	34	γ_1	52	SE _p
17	λ_3	35	γ_2		
18	p_1	36	γ_3		

Table 2. Descriptors and corresponding channels of the PolSAR multichannel image

3.3 Image segmentation results

The multi-resolution segmentation was used to delineate image objects and extract their features. The scale parameter determines the maximum change in heterogeneity that may occur when merging two image objects. Adjusting of the value of scale parameter influences the average object size. A larger value leads to bigger objects and vice versa. The optimal scale parameters for the multi-resolution segmentation were found according to some experiments. The corresponding segmentation results related to different segmentation scale parameters are shown in Figure 3. The segmentation with a scale of 10 was enough to delineate accurate land parcels.

Since the combined image consists of 52 channels, the number of features that can be extracted from one single object is as

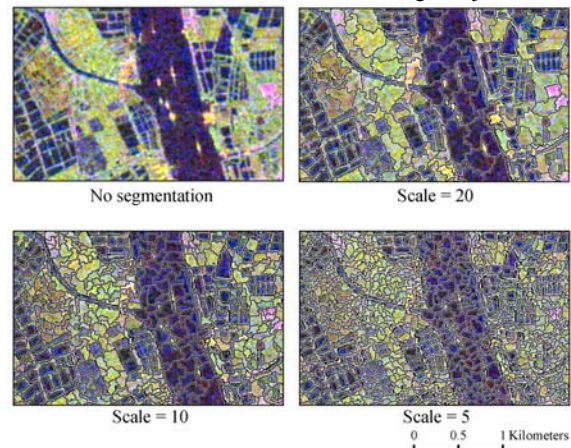


Figure 3. Determining the optimal scale for segmentation of Radarsat-2 image.

high as 1253. These features are the indigenous parameters of Definiens Developer 7.0, and they are listed as the following four major categories:

- 1) 208 (4×52) indicators related to the statistical values of each object: min, max, mean, and standard deviation of each layer;
- 2) 624 (12×52) indicators related to texture (e.g., Grey-level co-occurrence matrix (GLCM) Homogeneity, GLCM Contrast, GLCM Dissimilarity, and GLCM Entropy);
- 3) 364 (7×52) indicators related to spatial relationship (e.g., mean difference to neighbors, and mean difference to brighter neighbors);
- 4) 57 indicators related to shape (e.g., area, length, number of segments, and curvature/length (only main line) were extracted from an object;

3.4 Land use and land cover classification results

The classification maps using the proposed method and the Wishart supervised classification were produced as the comparison (Figure 4). The Wishart supervised classification was implemented by using the PolSARPro 4.0 software (López-Martínez, 2005).

3.5 Accuracy evaluation

Accuracy evaluation was carried out based on field investigation. The accuracy statistics of these two methods were produced in Table 5 and 6. The overall accuracy of our method was 89.34%, which was much higher than the Wishart supervised classification method, with an overall accuracy of 79.36%. Moreover, the overall kappa accuracy was also increased from 72.41% to 85.76% by using this proposed approach. The commission and omission errors can be measured by the user's and procurer's accuracy. The proposed method distinguished each class better than the Wishart supervised classification did, especially for identifying the built-up area. In the Wishart supervised classification, the accuracy of the user for the built-up area is very poor (50.28%). In this proposed method, however, the user's accuracy of the built-up area was much higher (77.84%). In the classification, industrial buildings with wide flat roof were commonly confused with barren land because of similar scattering mechanism. Some shadow of buildings was also prone to be classified as barren land. Otherwise, some buildings that have specific orientations not aligned in the azimuth direction or have complex structures

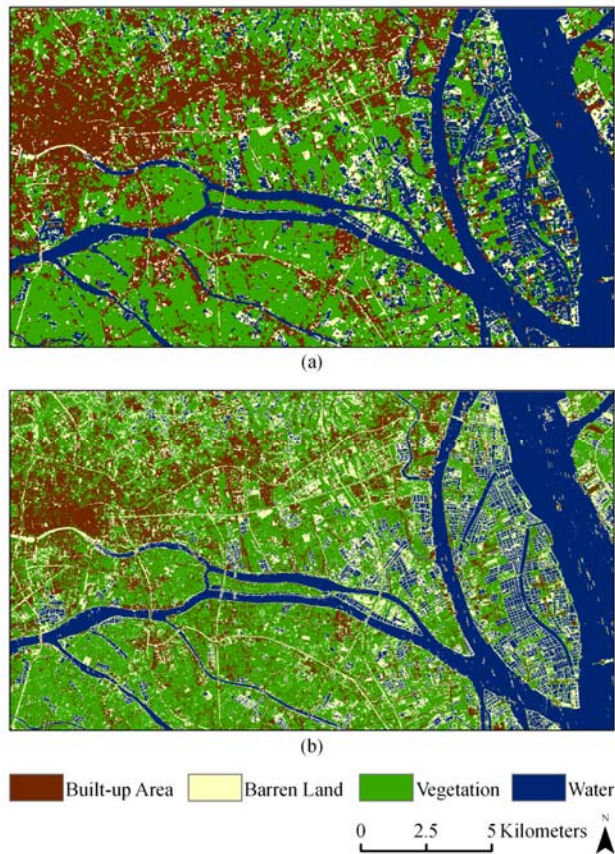


Figure 4. Land use and land cover classification results (a) Proposed method, (b) Wishart supervised classification.

such as rough roofs were assimilated into volume scattering class and then assigned to the vegetation class. In some mountain area covered with vegetation, some shadow was also prone to be classified as barren land. Barren lands with water on

their surface or high soil moisture were misclassified as water in the classification result. Some polluted water areas were also assigned to the barren land.

4. CONCLUSIONS

This paper proposed a new method that integrates polarimetric decomposition, object-oriented image analysis, and decision tree algorithms. The comparison between the proposed method and the Wishart supervised classification method indicates that the proposed method outperforms the Wishart supervised classification method, and can reduce discontinuous phenomenon effectively. The results show that the overall classification accuracy of the proposed method was 89.34% whereas it was 79.36% in the Wishart supervised classification method. Moreover, the overall kappa accuracy of the proposed method was also higher than that of the Wishart supervised classification method. The object-oriented image analysis is the suitable image processing method for information extraction to support the classification of polarimetric SAR images. Decision tree algorithms are efficient tools for the object-oriented classification of polarimetric SAR image. The experiments have indicated that the proposed method is an appropriate method for LULC classification of polarimetric SAR imagery.

REFERENCES

- Alberga, V., 2007. A study of land cover classification using polarimetric SAR parameters. *International Journal of Remote Sensing*, 28(17), pp. 3851-3870.
- Barnes, C. F. and Burki, J., 2006. Late-season rural land-cover estimation with polarimetric-SAR intensity pixel blocks and sigma-tree-structured near-neighbor classifiers. *IEEE Transactions on Geoscience and Remote Sensing*, 44(9), pp. 2384-2392.

Classification data	Reference data					User's Accuracy (%)
	Water	Vegetation	Built-up Area	Barren Land	Total	
Water	1,888	0	0	32	1,920	98.33
Vegetation	0	1,838	66	16	1,920	95.73
Built-up Area	19	234	1,370	137	1,760	77.84
Barren Land	173	86	39	1,622	1,920	84.48
Total	2,080	2,158	1,475	1,807	7,520	
Producer's accuracy (%)	90.77	85.17	92.88	89.76		
Overall accuracy (%)	89.34					
Overall kappa accuracy (%)	85.76					

Table 5. Classification accuracy (%) of the proposed method

Classification data	Reference data					User's Accuracy (%)
	Water	Vegetation	Built-up Area	Barren Land	Total	
Water	1,877	0	0	43	1,920	97.76
Vegetation	0	1,590	250	80	1,920	82.81
Built-up Area	2	666	885	207	1,760	50.28
Barren Land	221	44	39	1,616	1,920	84.17
Total	2,100	2,300	1,174	1,946	7,520	
Producer's accuracy (%)	89.38	69.13	75.38	83.04		
Overall accuracy (%)	79.36					
Overall kappa accuracy (%)	72.41					

Table 6. Classification accuracy (%) of the Wishart supervised classification

- Benz, U. C., Hofmann, P., Willhauck, G., Lingenfelder, I. and Heynen, M., 2004. Multi-resolution, object-oriented fuzzy analysis of remote sensing data for GIS-ready information. *ISPRS Journal of Photogrammetry and Remote Sensing*, 58, pp. 239-258.
- Cameron, W. L. and Rais, H., 2006. Conservative polarimetric scatterers and their role in incorrect extensions of the Cameron decomposition. *IEEE Transactions on Geoscience and Remote Sensing*, 44(12), pp. 3506-3516.
- Chen, K. S., Huang, W. P., Tsay, D. H. and Amar, F., 1996. Classification of multifrequency polarimetric SAR imagery using a dynamic learning neural network. *IEEE Transactions on Geoscience and Remote Sensing*, 34(3), pp. 814-820.
- Cloude, S. R. and Pottier, E., 1996. A review of target decomposition theorems in radar polarimetry. *IEEE Transactions on Geoscience and Remote Sensing*, 34(2), pp. 498-518.
- Cloude, S. R. and Pottier, E., 1997. An entropy based classification scheme for land applications of polarimetric SAR. *IEEE Transactions on Geoscience and Remote Sensing*, 35(1), pp. 68-78.
- Congalton, R. and Green, K., 1999. Assessing the Accuracy of Remotely Sensed Data: Principles and Practices. CRC Press, Boca Raton, pp. 74-79.
- Evans, C., Jones, R., Svalbe, I. and Berman, M., 2002. Segmenting multispectral Landsat TM images into field units. *IEEE Transactions on Geoscience and Remote Sensing*, 40(5), pp. 1054-1064.
- Ferro-Famil, L., Pottier, E. and Lee, J. S., 2001. Unsupervised classification of multifrequency and fully polarimetric SAR images based on the H/A/Alpha-Wishart classifier. *IEEE Transactions on Geoscience and Remote Sensing*, 39(11), pp. 2332-2342.
- Freeman, A. and Durden, S. L., 1998. A three-component scattering model for polarimetric SAR data. *IEEE Transactions on Geoscience and Remote Sensing*, 36(3), pp. 963-973.
- Friedl, M. A. and Brodley, C. E., 1997. Decision tree classification of land cover from remotely sensed data. *Remote Sensing of Environment*, 61(3), pp. 399-409.
- Geneletti, D. and Gorte, B. G. H., 2003. A method for object-oriented land cover classification combining Landsat TM data and aerial photographs. *International Journal of Remote Sensing*, 24(6), pp. 1273-1286.
- Huynen, J. R., 1970. Phenomenological theory of radar targets. *PhD dissertation*. Drukkerij Bronder-offset N. V., Rotterdam.
- Laliberte, A. S., Koppa, J., Fredrickson, E. L. and Rango, A., 2006. Comparison of nearest neighbor and rule-based decision tree classification in an object-oriented environment. *2006 IEEE International Geoscience and Remote Sensing Symposium*, Vols 1-8, 3923-3926.
- Langford, W. T., 2002. *Evaluation Functions in Aerial Image Segmentation*, Umi Proquest Digital Dissertations, Oregon State University, pp. 50-84.
- Lawrence, R. L. and Wright, A., 2001. Rule-based classification systems using classification and regression tree (CART) analysis. *Photogrammetric Engineering and Remote Sensing*, 67(10), pp. 1137-1142.
- Lee, J. S., Grunes, M. R., Ainsworth, T. L., Du, L. J., Schuler, D. L. and Cloude, S. R., 1999. Unsupervised classification using polarimetric decomposition and the complex Wishart classifier. *IEEE Transactions on Geoscience and Remote Sensing*, 37(5), pp. 2249-2258.
- Lee, J. S. and Pottier, E., 2009. *Polarimetric Radar Imaging from Basics to Applications*. (p. 180). CRC Press, New York.
- Li, X. and Yeh, A. G., 2004. Multi-temporal SAR images for monitoring cultivation systems using case-based reasoning. *Remote Sensing of Environment*, 90(4), 524-534.
- Li, H. T., Gu, H. Y., Han, Y. S. and Yang, J. H., 2008. Object-oriented classification of polarimetric SAR imagery based on statistical region merging and support vector machine. *2008 International Workshop on Earth Observation and Remote Sensing Applications*, pp. 147-152.
- Loh, W. Y. and Shih, Y. S., 1997. Split selection methods for classification trees. *Statistica Sinica*, 7(4), pp. 815-840.
- López-Martínez, C., Ferro-Famil, L., and Pottier, E., 2005. PolSARpro v4.0 Polarimetry Tutorial. <http://earth.esa.int/polsarpro/tutorial.html>.
- Mccoy, R.M., 2005, *Field Methods in Remote Sensing*. The Guilford Press, New York.
- McIver, D. K. and Friedl, M. A., 2002. Using prior probabilities in decision-tree classification of remotely sensed data. *Remote Sensing of Environment*, 81, pp. 253-261.
- Pottier, E. and Lee, J. S., 2000. Application of the "H/A/Alpha" polarimetric decomposition theorem for unsupervised classification of fully polarimetric SAR data based on the Wishart distribution. *CEOS SAR Workshop*, Toulouse, France, 450, pp. 335-340.
- Rignot, E., Chellappa, R. and Dubois, P., 1992. Unsupervised segmentation of polarimetric SAR data using the covariance-matrix. *IEEE Transactions on Geoscience and Remote Sensing*, 30(4), pp. 697-705.
- Swain, P. H. and Hauska, H., 1977. Decision tree classifier: design and potential. *IEEE Transactions on Geoscience and Remote Sensing*, 15(3), pp. 142-147.
- Yang, J., Yamaguchi, Y., Yamada, H., Sengoku, M. and Lin, S. M., 1998. Stable decomposition of mueller matrix. *IEICE Transactions on Communications*, E81-B(6), pp. 1261-1268.

ACKNOWLEDGEMENT

This work was supported by the Science and Operational Applications Research for RADARSAT-2 Program (SOAR 2762). The authors would like to thank MDA GEOSPATIAL SERVICES INC., Canada for providing the RADARSAT-2 data.